Applied Surface Science 623 (2023) 156986

Contents lists available at ScienceDirect

Applied Surface Science

journal homepage: www.elsevier.com/locate/apsusc

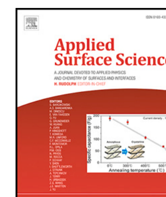

Full length article

Evidence of silicide at the Ni/β-Si_3N_4(0001)/Si(111) interface

Piu Rajak [a,b], Regina Ciancio [a,c], Antonio Caretta [d], Simone Laterza [d,e], Richa Bhardwaj [d], Matteo Jugovac [f], Marco Malvestuto [d,a], Paolo Moras [f], Roberto Flammini [g,*]

[a] CNR-IOM, Consiglio Nazionale delle Ricerche Istituto Officina dei Materiali, Trieste, Italy
[b] Abdus Salam International Centre for Theoretical Physics, Via Beirut, 6, 34151, Trieste, Italy
[c] Area Science Park Basovizza S.S. 14 Km 163.5 34149 Trieste, Italy
[d] Elettra Sincrotrone Trieste S.C.p.A. Strada Statale 14 - km 163.5 in AREA Science Park 34149 Basovizza, Trieste, Italy
[e] Department of Physics, University of Trieste, Via A. Valerio 2, 34127 Trieste, Italy
[f] CNR-ISM, Consiglio Nazionale delle Ricerche Istituto di Struttura della Materia, SS 14 km 163.5, I-34149, Trieste, Italy
[g] CNR-ISM, Consiglio Nazionale delle Ricerche Istituto di Struttura della Materia, Via del Fosso del Cavaliere 100, I-00133 Roma, Italy

ARTICLE INFO

Keywords:
β silicon nitride
Silicide
Metal/silicon interface
HRTEM
HAADF-STEM
EDS

ABSTRACT

We present a study of a sub-nanometre interlayer of crystalline silicon nitride at the Ni/Si interface. We performed transmission electron microscopy measurements complemented by energy dispersive X-ray analysis to investigate to what extent the nitride layer act as a barrier against atom diffusion. The results show that discontinuous silicide areas can form just below the nitride layer, whose composition is compatible with that of the nickel disilicide. The Ni–Si reaction is tentatively attributed to the thermal strain suffered by the interface during the deposition of Ni at low temperature.

1. Introduction

The increasing demand of the semiconductor industry for shrinking the size of physical components while improving density and performance, still keeps the spotlight of the condensed matter research on the properties of the metal/semiconductor interfaces [1]. In particular, magnetic metal/silicon interfaces are experiencing a renewed interest because of possible applications related to spintronics. For example, spin injection from a magnetic metal to a semiconductor [2] is expected to be at the bottom of electron spin-based future devices [3,4]. The description of these interfaces at the atomic level is therefore of paramount importance. This is why we undertook a study of the structural and chemical properties of a prototypical metal/semiconductor interface, namely the Ni/Si interface. So far, the research on this system was focused on the effort to guide the formation of stable silicides hosting suitable properties [5–7], despite being impossible to avoid interface reactions [5,8,9]. Nevertheless, attempts to prevent or delay the formation of silicides were also made [8].

Among the passivation layers used to avoid mass transfer across the interface, a thick layer of silicon nitride was often used, mainly in its amorphous phase [10]. In the present study, we explore the behaviour of a sub–nanometre thin crystalline layer of β silicon nitride at the Ni/Si interface. This insulator interlayer draws attention because of the negligible lattice mismatch with the (111) plane of the substrate. The difference between the surface lattice parameter of the 2 × 2 surface cell of Si(111) and the 1 × 1 cell of the β–Si_3N_4(0001) is indeed only 1.2% [11–13]. As a result, negligible mechanical strain is expected at the interface with silicon. Several studies about metals grown on the β–Si_3N_4/Si(111) interface have been reported in the literature, such as Au [14], Fe [15], Co [16–18], Ag [19] or Al [20], showing the ability to prevent the reaction with the silicon, except at temperatures higher than 500 K [17,21]. Ni seems to be an exception as it penetrates the nitride [8] or the oxide [22] interlayer even at room temperature (RT).

In the case of the Ni/Si interface, when Ni diffuses interstitially into the Si substrate, it is widely known that the temperature of the reaction significantly affects the formation of the Ni silicide phase [5]. The Ni_2Si phase initially forms during the silicide formation process in the range of temperatures from 200 °C to 280 °C [23], while NiSi (orthorhombic MnP-type) formation starts at about 350 °C [24]. Finally, the $NiSi_2$ phase forms when the temperature reaches 750 °C [25–28]. However, there are reports of a low-temperature formation of the $NiSi_2$ phase (below 500 K [29–35]) and due to the small lattice mismatch with Si (0.4%), epitaxial growth of $NiSi_2$ on Si can also be promoted even at RT [36,37].

In this study, we present a TEM (Transmission Electron Microscopy) study of the Ag/Ni/β–Si_3N_4/Si(111) interface, where the possible formation of silicides is investigated. We observe extended regions of $NiSi_2$

* Corresponding author.
E-mail address: roberto.flammini@cnr.it (R. Flammini).

https://doi.org/10.1016/j.apsusc.2023.156986
Received 23 November 2022; Received in revised form 2 March 2023; Accepted 8 March 2023
Available online 13 March 2023
0169-4332/© 2023 Elsevier B.V. All rights reserved.

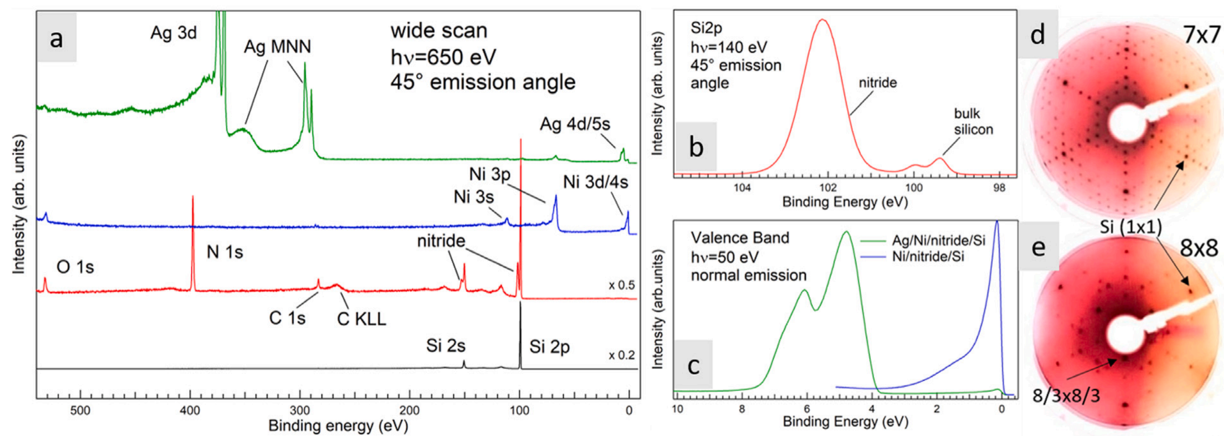

Fig. 1. Panel (a), photoemission survey scans taken at 650 eV photon energy. The spectra have been recorded on the bare Si surface (black), after nitridation (red), after growth of 20 nm of Ni (blue) and after growth of the silver capping layer (green). In panel (b) the Si2p core level spectrum taken at 140 eV photon energy is shown, recorded in surface sensitive conditions. In panel (c), the valence band spectra after Ni and Ag growth are displayed in blue and green, respectively. The Fermi level is located at 0 eV binding energy. Panels (d) and (e) show the LEED patterns taken at 58 eV primary electron energy, on the (7 × 7)– and (8 × 8)–reconstructed surfaces, respectively. The colours have been inverted so as to better highlight the diffraction spots.

with well-defined thickness and stoichiometry, separated by regions of lower Ni concentration. This finding is attributed to the presence of cracks in the nitride layer possibly due to the different thermal expansion coefficients of Si and β–Si_3N_4 at low temperature.

2. Experiment

A Si(111)–p(B) sample (resistivity ρ=0.05 Ω cm) was used as a substrate to thermally grow a layer of silicon nitride. In order to ascertain the cleanliness and the degree of atomic order at the surface we induced the 7 × 7 surface reconstruction by repeated flashes at high temperature (1500 K). The surface was then exposed to an ammonia flux (100 L) while keeping the sample at about 1050 K. This preparation ensured the growth of a couple of bilayers of crystalline β–silicon nitride, as well known from the literature [12,13].

Ni was deposited in UHV (Ultra High Vacuum), by using an effusion cell calibrated with a quartz microbalance. The deposition rate was 0.6 ML per minute, where 1 ML Ni is equal to 2 Å which is the interlayer distance along the (111) direction. Nickel was deposited by using the two-step growth, in which firstly the adsorbate was grown at low temperature (100 K) and then it was left recovering the RT. This protocol guarantees the formation of a flat Ni layer [38–40], avoiding the Volmer–Weber growth mode occurring at RT [15–17,20,41–43]. In our experiment we prepared Ni films of 7 and 20 nm thickness. The Ni/nitride/Si interface was then covered by 2 nm of Ag grown with an effusion cell at RT, in order to reduce the contamination by the ambient air caused by the transport to the vacuum chamber hosting the microscope. The sample preparation and the measurements were performed at the VUV-Photoemission Beamline of the Elettra Synchrotron Radiation Source, Italy. The spectra were acquired at RT, with photon energies of 650, 140 and 50 eV, using a Scienta R-4000 electron analyser.

High resolution TEM (HRTEM) and high angle annular dark field (HAADF) scanning TEM (STEM) investigations were carried out on cross-sectional samples by using a JEOL 2010 UHR field emission gun microscope operated at 200 kV with a determined spherical aberration coefficient Cs of 0.47 ± 0.01 mm. The microscope is equipped with an Oxford system for Energy-Dispersive X-ray Spectroscopy (EDS) studies. HAADF STEM images were acquired using an illumination angle of 12 mrad and a collection angle 88 $\le 2\theta \le$ 234 mrad. To precisely determine the elemental chemical profiles over the interfacial region, EDS analyses were carried out in STEM mode using 0.5 nm electron probe. Conventional mechanical polishing followed by dimpling and ion etching with Ar-gas were used to prepare cross-sectional TEM specimens.

3. Results

3.1. Photoemission spectra

In panel (a) of Fig. 1, XPS survey spectra of the interface with 20 nm of Ni are displayed. We only show the spectra for the thick sample as no additional information is gathered from the spectrum taken on the thinner one. At the bottom of panel (a) the spectrum relative to the bare silicon surface is displayed. Apart from the presence of the nitrogen and silicon core level peaks, the typical fingerprint of the presence of the nitride is noticeable: beside the Si2p and the Si2s core levels another peak at higher binding energy is present and is attributed to the Si-N bonds [12,14]. The N1s peak cannot show the nitride related contribution due to the small chemical shift [12,17]. The spectrum taken on the nitride surface appears slightly contaminated by carbon and oxygen. These chemical species show different behaviours with respect to the subsequent Ni and Ag deposits: the oxygen floats on top of the nickel and of the silver surfaces, while the carbon remains buried at the interface. At first glance, the spectra do not show any formation of nickel silicides [44] as the short photoelectron escape depth prevents their identification. As a matter of fact, more bulk sensitive techniques need to be used, as photoemission is primarily sensitive to the first few layers of the sample. To avoid any possible misinterpretation of the results, the data shows that no contamination from other chemical species (except for O or C) is present. In panel (b), the high resolution Si2p core level spectrum is displayed. Bulk silicon and silicon nitride components are observed, in perfect agreement with the literature [12,14,17,21,43]. In panel (c) we show valence bands taken after deposition of the Ni and of the Ag layers. From the comparison with the literature, it is evident that the oxidation of the Ni and Ag surfaces is negligible [45,46]. In panels (d) and (e) LEED (Low Energy Electron Diffraction) patterns taken on the Si(111)-(7 × 7) and β–Si_3N_4–(8 × 8) reconstructed surfaces are displayed. The "8/3 × 8/3" order spots are generally attributed to the topmost N adatoms of the surface superstructure, making certain the formation of the correct β–Si_3N_4/Si(111) interface [47,48]. The Si(111)–(1 × 1) spots are also indicated on both reconstructions as a reference.

3.2. TEM analysis

Fig. 2 shows a representative cross-sectional bright field TEM micrograph of the Ag/Ni/β–Si_3N_4/Si(111) heterostructure with various thicknesses of the Ni thin film, namely with 7 nm (Fig. 2a) and 20 nm (Fig. 2b). The corresponding intensity line profiles obtained from the

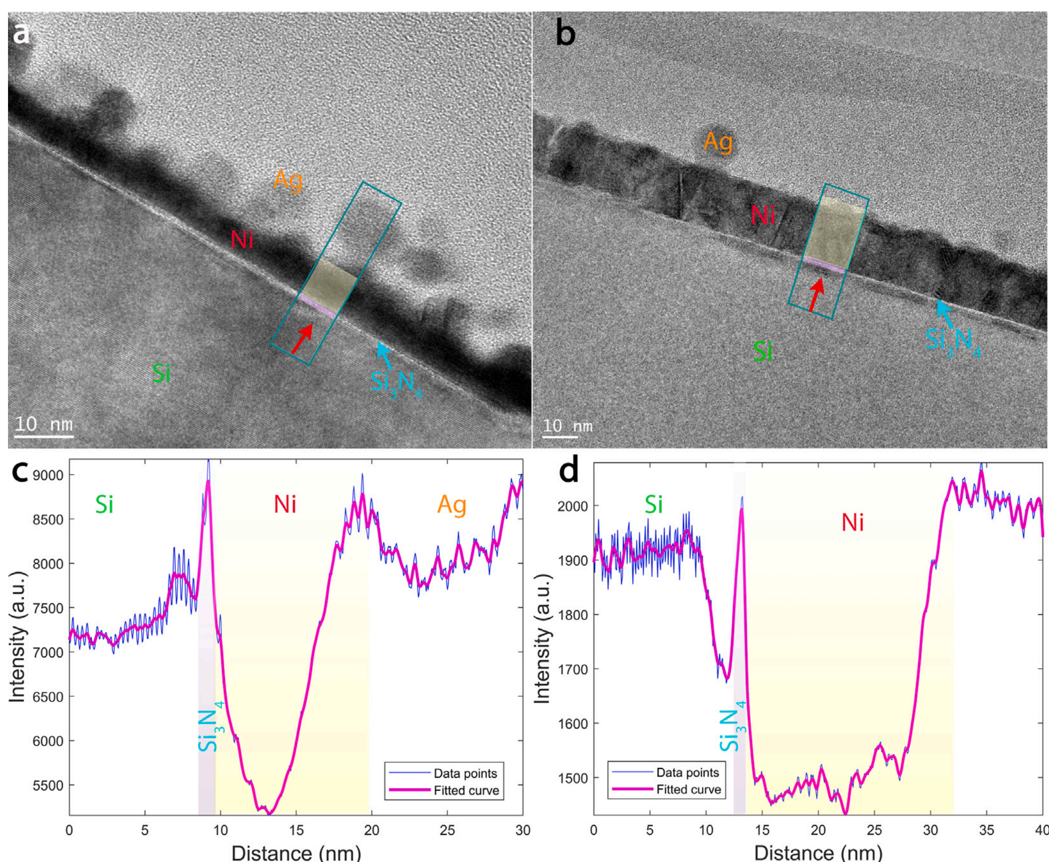

Fig. 2. Overview TEM micrograph of the two heterostructures with (a) 7 nm Ni, (b) 20 nm Ni. Corresponding intensity line profiles are collected from the cyan coloured box region and shown in (c) for 7 nm Ni, (d) 20 nm Ni. The grey round features are ascribed to the silver capping layer.

marked region of interest are depicted in Figs. 2c and d, respectively. The phase contrast imaging allows us to identify a thin and continuous Si_3N_4 epilayer which homogeneously extends on top of the bare Si substrate with a thickness of about 0.8 nm, as enlightened by the intensity profiles (magenta coloured region). Traces of Ag capping layer used to prevent the Ni layer from oxidation can also be noted on the film's surface. Silver particles with diameters up to 10 nm suggest the possible increase of the local temperature inducing a dewetting process.

Further information on the structural properties of the films was obtained by HRTEM. Fig. 3 displays representative HRTEM images of the (a) 7 nm- and (b) 20 nm-thick Ni film heterostructures acquired along the [110] zone axis of the Si substrate. We stress here the ability of the two-step growth process to produce a nearly flat Ni layer, which is in agreement with the cases of either aluminium or silver [19,49]. In the HRTEM image of 20 nm thick Ni film heterostructure (Fig. 3b), the interplanar lattice spacings of silicon nitride and Si have been measured and found to be of about 2.9 Å within the silicon nitride layer and 3.3 Å within the Si substrate, which correspond to the interplanar distances of the β–Si_3N_4 [50] and Si(111) [51], respectively. The corresponding Fast-Fourier Transforms (FFT) of the 7 nm-thick and 20 nm-thick Ni films are presented in the insets of Figs. 3a and 3b, clearly revealing the polycrystalline nature of the Ni film. The diffraction ring with lattice spacing 2.0 Å corresponds to the (111) plane of Ni with cubic structure. The dark contrast region between the Si substrate and the silicon nitride layer (Fig. 3d) displays an interplanar distance of about 3.1 Å which is compatible with the $NiSi_2$ phase. From the FFT of the area located across the dark region below the silicon nitride layer, we extracted lattice spacings of 3.1 Å and 1.9 Å, compatible with the (11-1) and (02-2) planes of the $NiSi_2$ phase [52], respectively. Our measurements provide no evidence of the Ni_2Si phase. Moreover, by careful inspection of β–Si_3N_4/Ni interface (Fig. 3c), the difference in sharpness of the interface can be noticed. For ease of visualization, the interface has been divided in three regions (marked as I, II and III). Region II appears sharper than regions I and III. Additionally, a varying diffraction contrast of the β–Si_3N_4 layer along the interface is visible, so that the formation of the silicide phase below the β–Si_3N_4 layer can be associated with the presence of a discontinuity occurring at the nitride layer.

The chemical nature of the two heterostructures was elucidated by the HAADF-STEM imaging. Representative HAADF-STEM micro-graphs of the 7 nm- and 20 nm-thick Ni layer are shown in Figs. 4a and 4b, respectively. The setup for HAADF-STEM produces images whose contrast is approximately proportional to the square of the average atomic number of the illuminated area and to the thickness of the specimen [53,54]. In both heterostructures, HAADF-STEM provides evidence of four regions (marked as S, A, B, and C in Figs. 4a and 4b) with different chemical contrast, the darker contrast region being associated with the substrate (region S) while brighter contrast corresponds to the Ni film (region C). The dark contrast epilayer of about 0.8 nm right below the Ni film (region B) can be attributed to the Si_3N_4 continuous layer already observed by HRTEM. In addition, a well defined 3 nm-thick layer (region A) is visible at the interface between the Si_3N_4/Ni heterostructure and the Si substrate. The contrast of this layer (brighter with respect to the Si substrate and darker compared to the Ni film) indicates a higher average atomic number compared to the Si substrate and lower than the Ni film, which is compatible with chemical inter-diffusion occurring across the interfaces. Contrast drops can also be seen along the region A (indicated by white arrows in the figure), which can be attributed to the regions where the silicon nitride layer is continuous. For ease of visualization, the intensity profiles are overlaid on the corresponding images to heighten the contrast variations across the heterostructures.

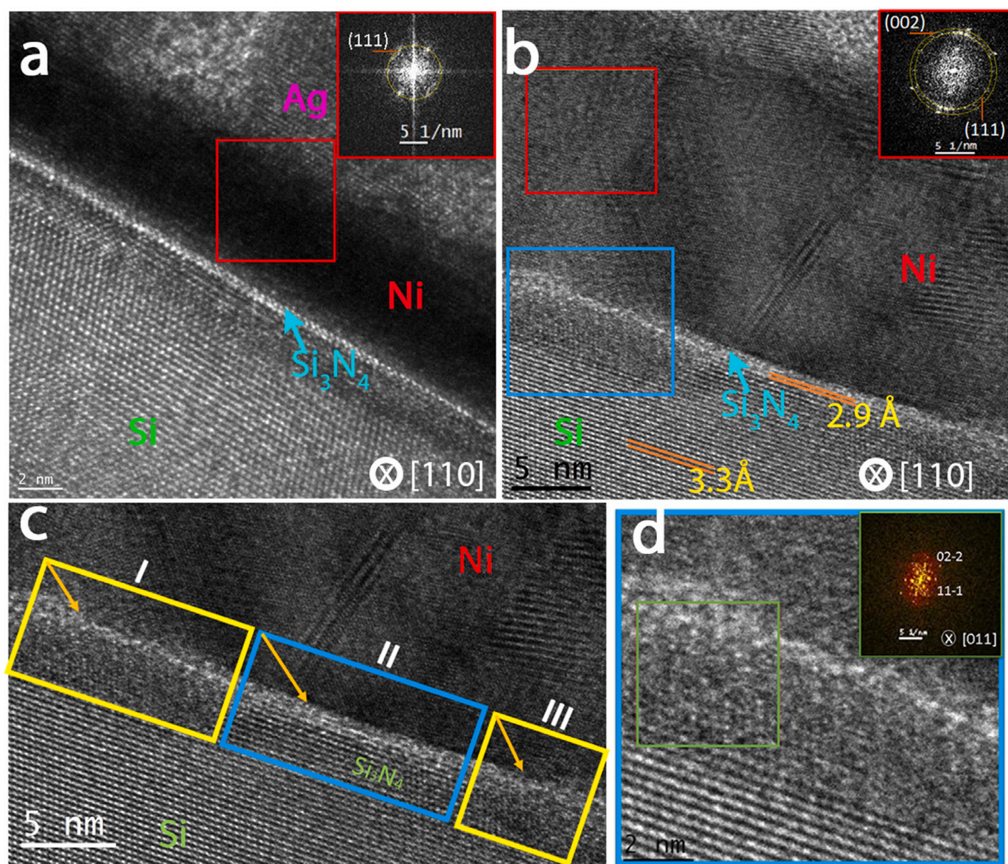

Fig. 3. HRTEM images of two heterostructures with (a) 7 nm Ni and (b) 20 nm Ni. The crystalline order across the whole interface is noticed. The insets display the FFTs extracted from the red square regions within the Ni layer, showing its polycrystalline growth. In panel (c) the comparison between the interface region II (pointed with arrow) and regions I and III is displayed, showing the presence of a defect in the nitride layer. In panel (d) the enlarged area of the region of panel (b) is marked in blue. The insets show FFTs extracted from the green square area within the region between the nitride layer and Si substrate. Diffraction spots represent the $NiSi_2$ phase, with lattice spacing (11-1) and (02-2).

To further elucidate the chemical nature of the two heterostructures, we performed an EDS analysis. The EDS was carried out in STEM mode by scanning an electron probe of 0.5 nm to precisely determine the elemental chemical profiles across the interfacial region. Si K- and Ni K-shell elemental profiles collected perpendicularly to the interface of the 7 nm- and 20 nm-thick Ni film heterostructures are displayed in Fig. 4. In both cases, the elemental profiles show the existence of an intermixed region at the substrate/film interface (region A) of about 3 nm thickness where both Ni and Si signals are detected. Quantitative information on the chemical composition of region A was obtained by a set of EDS spectra collected from adjacent areas of region A in the HAADF-STEM image of Fig. 5. The quantitative EDS results (summarized in Table 1) are compatible with a Si:Ni = 2:1 stoichiometric ratio corresponding to the formation of the $NiSi_2$ phase, which is the most common and stable silicide at the Ni/Si(111) interface [44,55]. The EDS analyses provide no evidence of a Ni-rich silicide (Ni_2Si) phase, thus confirming the HRTEM results. Our finding is in good agreement with Ref. [55] which reports that the formation of voids in SiO_2 layer allows Ni atoms to migrate into the Si substrate and initiate additional solid-state reactions, creating crystals of $NiSi_2$. Furthermore, the formation of a ternary compound, such as Ni–Si–N can be ruled out at RT, as the ternary phase diagram excludes this possibility except for very high temperatures [56,57]. This agrees with the case of gold [21].

Quantitative EDS within the region B is limited by beam broadening effects, taking into account that the 0.5 nm probe size of the EDS in STEM mode is very close to the 0.8 nm thickness of the Si_3N_4 region. In addition, due to the very low Z number, nitrogen cannot not be detected in layer B. However, the darker Z-contrast and continuity of region B are in a very good agreement with the nanostructure of the atomically sharp layer clearly detected by phase contrast imaging (Fig. 3). The Ni signal is clearly predominant in region C. The presence of Si can also be detected, although this can be attributed to re-deposition coming from TEM specimen preparation.

Table 1
Atomic percentage of Si and Ni observed in region A of Fig. 5. The total percentage for each site amounts to 100%. The labels refer to the areas where the EDS spectra have been collected.

Site	1	2	3	4	5	6
Si	69.3	64	66.2	61.7	67.7	62.4
Ni	30.7	36	33.8	38.3	32.3	37.6

The results presented above show evidence of mass transport at the Ni/β–Si_3N_4/Si(111) as reported in the literature [65], although the nitridation protocol in the above paper involved a plasma reactor (more susceptible of contamination due to the working pressure being much higher than the usual UHV chambers). The nitride layer does not show a manifest disruption of its structure so that pits, defects or cracks at the interface can be at the origin of the atomic diffusion. In the case of the interface made with gold [21], the silicon segregation and the gold diffusion in the silicon substrate was demonstrated only at higher temperatures. The reason why Ni behaves differently with respect to gold can be related to the ability of nickel to weaken the Si–N bond, as suggested also for cobalt at much higher temperatures [66].

In Ref. [67] the authors show the importance of the nitride growth conditions for the formation of defects and pits at the interface with

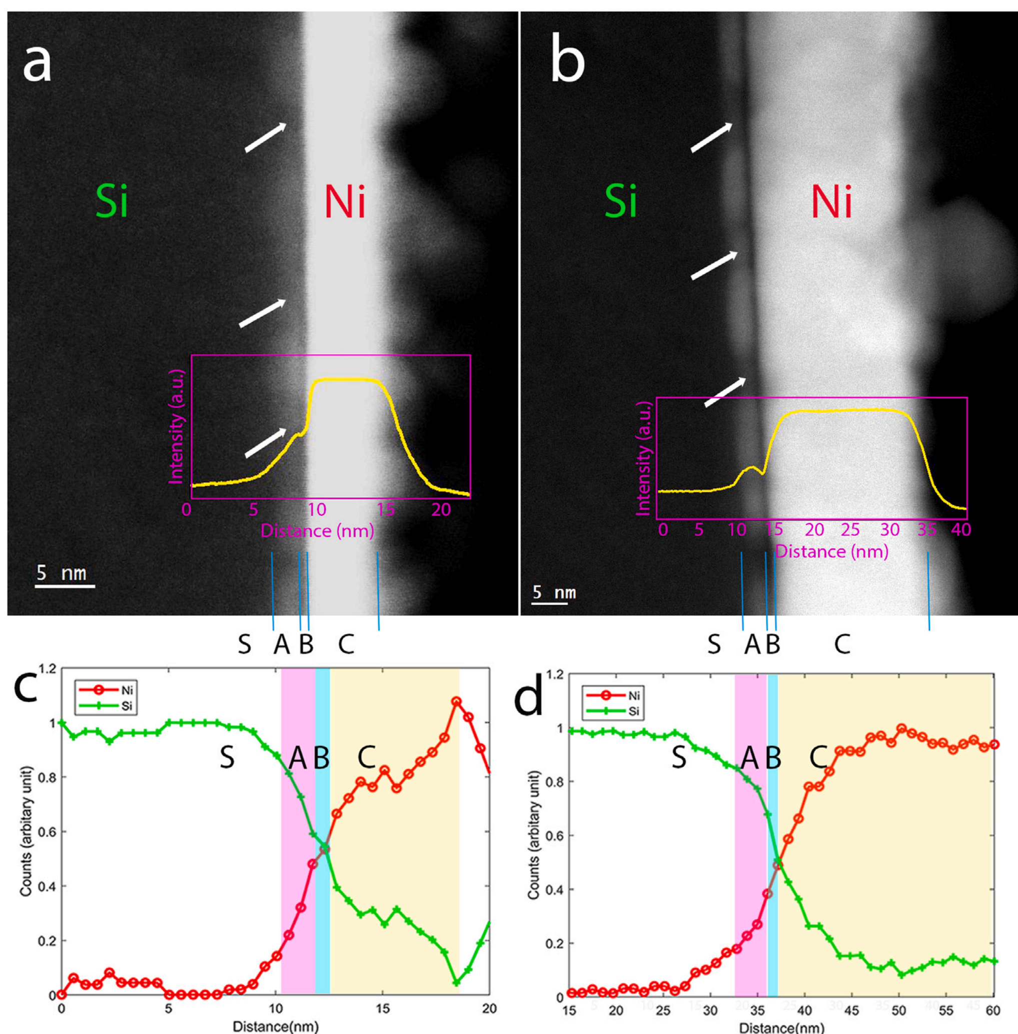

Fig. 4. HAADF-STEM images of two heterostructures with (a) 7 nm Ni, (b) 20 nm Ni. The white arrows points the continuous regions. The line profiles are overlaid on the image to indicate the contrast profile within the imaged region. From the intensity profiles, four regions named S, A, B, and C can be identified. The EDX elemental profiles are shown in panels (c) and (d) for heterostructures with 7 nm Ni and 20 nm Ni thickness, respectively.

Table 2
Comparison between linear thermal expansion coefficients ($10^{-6}K^{-1}$) of silicon, silicon nitride and nickel. The data refer to bulk crystalline structures. 100 K and 300 K are the temperatures at which the Ni deposition and the TEM experiments were carried out, respectively. The asterisk (*) refers to a value reported for 90 K.

T(K)	α_{Si}	Ref.	$\alpha_{\beta-Si3N4}$	Ref.	α_{Ni}	Ref.
100	−0.344	[58,59]	−0.20*	[60]	+65	[61]
300	+2.611	[58]	+3.0	[62]	+129	[61]
	+2.5	[59]	+4.5	[63]		
			+1.19	[64]		

Ni that are deleterious for the electronic structure of the interface. The very same structural defects or pitfalls in our case can be responsible for the atomic diffusion. This is also demonstrated by the discontinuous nature of the silicide: the Ni diffusion seems to be located at random positions below the nitride layer. This can also point to possible effects related to mechanical stress suffered by the interface during the Ni deposition at low temperature (100 K) and the following recovery of the RT. As shown in Table 2 the comparison among the thermal expansion coefficients of the silicon, silicon nitride and nickel shows indeed important differences. Although the data reported in the literature are scattered and refer to bulk isolated systems, the possibility cannot be ruled out that cracks can form due to the large temperature excursion: silicon and silicon nitride show a similar behaviour, as they contract at 100 K and expand at 300 K, while nickel only expands in the same temperature range. Nevertheless, a clear attribution of the reasons why silicides form still cannot be made.

4. Conclusion

We report on a sub-nanometre crystalline interlayer of β-silicon nitride at the Ni/Si interface. Nickel was deposited at low temperature so as to favour a layer by layer growth. A silver capping layer was deposited at RT to protect the surface from oxidation. By means of a TEM study complemented by EDS analysis and photoemission, we observed the presence of silicon on top of the interface and a migration of the nickel atoms within the silicon substrate. This is tentatively ascribed to the possible presence of cracks of the nitride layer induced by the low temperature reached during Ni deposition. The silicide

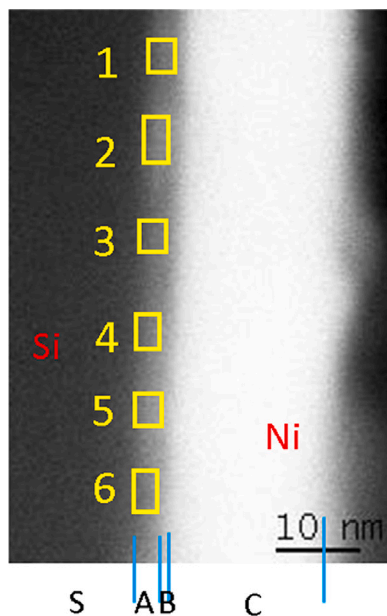

Fig. 5. HAADF STEM image of heterostructure. The areas selected for collecting the EDS spectra are indicated by rectangles.

region ranges 3 to 5 nm from the nitride edge and its chemical analysis suggests the formation of $NiSi_2$. The silver capping layer shows a contrasting behaviour as it both partly protects the nickel surface and partly forms particles of nanometric size.

CRediT authorship contribution statement

Piu Rajak: Conceptualization, Investigation, Data curation, Writing – original draft. **Regina Ciancio:** Conceptualization, Investigation, Data curation, Writing – original draft. **Antonio Caretta:** Conceptualization, Investigation, Writing – review & editing. **Simone Laterza:** Writing – review & editing. **Richa Bhardwaj:** Writing – review & editing. **Matteo Jugovac:** Writing – review & editing. **Marco Malvestuto:** Conceptualization, Data curation, Writing – review & editing. **Paolo Moras:** Conceptualization, Investigation, Data curation, Writing – review & editing. **Roberto Flammini:** Conceptualization, Investigation, Data curation, Writing – original draft.

Declaration of competing interest

The authors declare that they have no known competing financial interests or personal relationships that could have appeared to influence the work reported in this paper.

Data availability

Data will be made available on request.

Acknowledgements

This work has received funding from the EU-H2020 research and innovation programme under grant agreement no. 654360 having benefitted from the access provided by CNR-IOM in Trieste within the framework of the NFFA-Europe Transnational Access Activity (proposal ID334) and performed in the framework of the Nanoscience Foundry and Fine Analysis (NFFA-MIUR Italy Progetti Internazionali) facility. P. M. acknowledges EUROFEL-ROADMAP ESFRI of the Italian Ministry of Education, University, and Research. We would like to acknowledge Pasquale Orgiani at CNR-IOM for his valuable contributions and insightful discussions. E. Cociancich is gratefully acknowledged for the TEM specimen preparation. P.R. acknowledges the receipt of a fellowship from the ICTP Programme for Training and Research in Italian Laboratories, Trieste, Italy.

References

[1] IEEE, The international roadmap for devices and systems, More Moore, 2021 update, 2021, https://irds.ieee.org/editions/2021/more-moore.

[2] S. Laterza, A. Caretta, R. Bhardwaj, R. Flammini, P. Moras, M. Jugovac, P. Rajac, M. Islam, R. Ciancio, V. Bonanni, B. Casarin, A. Simoncig, M. Zangrando, P. Ribic, G. Penco, G. de Ninno, L. Giannessi, A. Demidovich, M. Danailov, F. Parmigiani, M. Malvestuto, All-optical spin injection in silicon investigated by element specific time-resolved Kerr effect, Optica 9 (2022) XX, http://dx.doi.org/10.1364/OPTICA.471951.

[3] G.A. Prinz, Magnetoelectronics, Science 282 (1998) 1660–1663, http://dx.doi.org/10.1126/science.282.5394.1660, URL https://www.science.org/doi/abs/10.1126/science.282.5394.1660.

[4] S.A. Wolf, D.D. Awschalom, R.A. Buhrman, J.M. Daughton, S. von Molnár, M.L. Roukes, A.Y. Chtchelkanova, D.M. Treger, Spintronics: A spin-based electronics vision for the future, Science 294 (2001) 1488–1495, http://dx.doi.org/10.1126/science.1065389, URL https://www.science.org/doi/abs/10.1126/science.1065389, arXiv:https://www.science.org/doi/pdf/10.1126/science.1065389.

[5] H. von Känel, Growth and characterization of epitaxial Ni and Co silicides, Mater. Sci. Rep. 8 (1992) 193–269, http://dx.doi.org/10.1016/0920-2307(92)90003-J, URL https://www.sciencedirect.com/science/article/pii/092023079290003J.

[6] R. Tung, Epitaxial CoSi2 and NiSi2 thin films, Mater. Chem. Phys. 32 (1992) 107–133, http://dx.doi.org/10.1016/0254-0584(92)90268-D, URL https://www.sciencedirect.com/science/article/pii/025405849290268D.

[7] R.T. Tung, J.M. Gibson, J.M. Poate, Formation of ultrathin single-crystal silicide films on Si: Surface and interfacial stabilization of Si-$NiSi_2$ epitaxial structures, Phys. Rev. Lett. 50 (1983) 429–432, http://dx.doi.org/10.1103/PhysRevLett.50.429, URL https://link.aps.org/doi/10.1103/PhysRevLett.50.429.

[8] A. Hiraki, Low temperature reactions at Si/metal interfaces; what is going on at the interfaces? Surf. Sci. Rep. 3 (1983) 357–412, http://dx.doi.org/10.1016/0167-5729(84)90003-7, URL https://www.sciencedirect.com/science/article/pii/0167572984900037.

[9] E.R. Weber, Transition metals in silicon, Appl. Phys. A 30 (1983) 1–22, http://dx.doi.org/10.1007/BF00617708.

[10] A.E. Kaloyeros, F.A. Jové, J. Goff, B. Arkles, Review—silicon nitride and silicon nitride-rich thin film technologies: Trends in deposition techniques and related applications, ECS J. Solid State Sci. Technol. 6 (2017) P691–P714, http://dx.doi.org/10.1149/2.0011710jss.

[11] X.S. Wang, G. Zhai, J. Yang, L. Wang, Y. Hu, Z. Li, J.C. Tang, X. Wang, K.K. Fung, N. Cue, Nitridation of Si(1 1 1), Surf. Sci. 494 (2001) 83–94, http://dx.doi.org/10.1016/S0039-6028(01)01409-1.

[12] J.W. Kim, H.W. Yeom, Surface and interface structures of epitaxial silicon nitride on Si(111), Phys. Rev. B 67 (2003) 035304, http://dx.doi.org/10.1103/PhysRevB.67.035304, URL http://link.aps.org/doi/10.1103/PhysRevB.67.035304.

[13] R. Flammini, P. Allegrini, F. Wiame, R. Belkhou, F. Ronci, S. Colonna, D.M. Trucchi, F. Filippone, S.K. Mahatha, P.M. Sheverdyaeva, P. Moras, Nearly-free electronlike surface resonance of a β–Si_3N_4(0001)/Si(111) interface, Phys. Rev. B 91 (2015) 075303, http://dx.doi.org/10.1103/PhysRevB.91.075303, URL https://link.aps.org/doi/10.1103/PhysRevB.91.075303.

[14] R. Flammini, R. Belkhou, F. Wiame, S. Iacobucci, A. Taleb-Ibrahimi, Crystalline silicon nitride passivating the Si(111) surface: A study of the Au growth mode, Surf. Sci. 579 (2005) 188–196, http://dx.doi.org/10.1016/j.susc.2005.02.005, URL http://www.sciencedirect.com/science/article/pii/S0039602805001391.

[15] K. Eguchi, Y. Takagi, T. Nakagawa, T. Yokoyama, Growth process and magnetic properties of iron nanoparticles deposited on Si_3N_4/Si(111)-(8 × 8), Phys. Rev. B 85 (2012) 174415, http://dx.doi.org/10.1103/{PhysRevB}.85.174415.

[16] S. Gwo, C.-P. Chou, C.-L. Wu, Y.-J. Ye, S.-J. Tsai, W.-C. Lin, M.-T. Lin, Self–limiting size distribution of supported cobalt nanoclusters at room temperature, Phys. Rev. Lett. 90 (2003) 185506, http://dx.doi.org/10.1103/PhysRevLett.90.185506.

[17] R. Flammini, F. Wiame, R. Belkhou, A. Taleb-Ibrahimi, P. Moras, Thermal stability of the Co/β-Si3N4/Si(111) interface: A photoemission study, Surf. Sci. 606 (2012) 1215, http://dx.doi.org/10.1016/j.susc.2012.03.023.

[18] F. Jiménez-Villacorta, A. Espinosa, E. Céspedes, C. Prieto, Magnetic properties and short-range structure analysis of granular cobalt silicon nitride multilayers, J. Appl. Phys. 110 (2011) http://dx.doi.org/10.1063/1.3665877.

[19] R. Flammini, S. Colonna, P.M. Sheverdyaeva, M. Papagno, A.K. Kundu, P. Moras, Effect of a subnanometer thin insulator layer at the Ag/Si(111) interface through the observation of quantum well states, Phys. Rev. Mater. 5 (2021) 084604, http://dx.doi.org/10.1103/PhysRevMaterials.5.084604, URL https://link.aps.org/doi/10.1103/PhysRevMaterials.5.084604.

[20] E. Khramtsova, A. Saranin, V. Lifshits, Chemical and structural transformations in the Al/Si(111)8 × 8-n system, Surf. Sci. 295 (1993) 319–324, http://dx.doi.org/10.1016/0039-6028(93)90278-R, URL http://www.sciencedirect.com/science/article/pii/003960289390278R.
[21] R. Flammini, F. Wiame, R. Belkhou, A. Taleb-Ibrahimi, C. Spezzani, P. Moras, C. Crotti, Thermal behavior of the Au/C-Si3N4/Si(111) interface, J. Appl. Phys. 103 (2008) 083528, http://dx.doi.org/10.1063/1.2907439.
[22] K. Honda, T. Nakanishi, Influence of Ni impurities at the Si-SiO2 interface on the metal–oxide–semiconductor characteristics, J. Appl. Phys. 75 (1994) 7394–7399, http://dx.doi.org/10.1063/1.356654.
[23] S. Lau, J. Mayer, K. Tu, Interactions in the Co/Si thin-film system. i. kinetics, J. Appl. Phys. 49 (1978) 4005–4010, http://dx.doi.org/10.1063/1.325359, cited by: 168.
[24] T. Finstad, A Xe marker study of the transformation of Ni2Si to NiSi in thin films, Phys. Status Solidi (A) 63 (1981) 223–228, http://dx.doi.org/10.1002/pssa.2210630130, URL https://www.scopus.com/inward/record.uri?eid=2-s2.0-0019392048&doi=10.1002%2fpssa.2210630130&partnerID=40&md5=82a3920e36dc6fa48ed844ffb18475ad.
[25] F. D'Heurle, S. Petersson, L. Stolt, B. Strizker, Diffusion in intermetallic compounds with the CaF2 structure: A marker study of the formation of NiSi2 thin films, J. Appl. Phys. 53 (1982) 5678–5681, http://dx.doi.org/10.1063/1.331453.
[26] F. D'Heurle, C.S. Petersson, J.E. Baglin, S.J. La Placa, C.Y. Wong, Formation of thin films of NiSi: Metastable structure, diffusion mechanisms in intermetallic compounds, J. Appl. Phys. 55 (1984) 4208–4218, http://dx.doi.org/10.1063/1.333021.
[27] D. Mangelinck, T. Luo, C. Girardeaux, Reactive diffusion in the presence of a diffusion barrier: Experiment and model, J. Appl. Phys. 123 (2018) http://dx.doi.org/10.1063/1.5023578.
[28] M. Dascalu, R. Levi, F. Cesura, O. Diéuez, I. Goldfarb, Interface effects on epilayer surface density of states by scanning tunneling spectroscopy and density functional theory, Adv. Theory Simul. 2 (2019) 1–12, http://dx.doi.org/10.1002/adts.201900140.
[29] A. Noya, M.B. Takeyama, Low-temperature formation of NiSi2 phase in Ni/Si system, Electron. Commun. Japan 99 (2016) 85–91, http://dx.doi.org/10.1002/ecj.11860.
[30] V. Teodorescu, L. Nistor, H. Bender, A. Steegen, A. Lauwers, K. Maex, J. Van Landuyt, In situ transmission electron microscopy study of Ni suicide phases formed on (001) Si active lines, J. Appl. Phys. 90 (2001) 167–174, http://dx.doi.org/10.1063/1.1378812.
[31] R.T. Tung, J.M. Gibson, J.M. Poate, Formation of ultrathin dingle-crystal silicide films on Si: Surface and interfacial stabilization of Si-NiSi2 epitaxial structures, Phys. Rev. Lett. 50 (1983) 429–432, http://dx.doi.org/10.1103/PhysRevLett.50.429.
[32] U. Göele, K.N. Tu, Growth kinetics of planar binary diffusion couples: Thin-film case versus bulk cases, J. Appl. Phys. 53 (1982) 3252–3260, http://dx.doi.org/10.1063/1.331028.
[33] N. Ikarashi, Atomic structure of a Ni diffused Si(001) surface layer: Precursor to formation of NiSi2 at low temperature, J. Appl. Phys. 107 (2010) 2–6, http://dx.doi.org/10.1063/1.3294691.
[34] R.D. Reus, H.C. Tissink, F.W. Saris, Low temperature epitaxial Nisi2 formation on Si(111) by diffusing Ni through amorphous Ni-Zr, J. Mater. Res. 5 (1990) 341–346, http://dx.doi.org/10.1557/JMR.1990.0341.
[35] C.L. Hsin, Y.S. Tsai, Epitaxial silicides: The case of Fe, Ni, and Ti, CrystEngComm 18 (2016) 8155–8158, http://dx.doi.org/10.1039/c6ce01375a.
[36] R. Tung, F. Schrey, Growth of epitaxial NiSi2 on Si(111) at room temperature, Appl. Phys. Lett. 55 (1989) 256–258, http://dx.doi.org/10.1063/1.102385, cited by: 42.
[37] T. Isshiki, K. Nishio, T. Sasaki, H. Harima, M. Yoshimoto, T. Fukada, W.S. Yoo, High-resolution transmission electron microscopy of interfaces between thin nickel layers on Si(001) after nickel silicide formation under various annealing conditions, 2006, pp. 121–125, http://dx.doi.org/10.1109/RTP.2006.367991, cited by: 4.
[38] G. Neuhold, K. Horn, Depopulation of the Ag(111) surface state assigned to strain in epitaxial films, Phys. Rev. Lett. 78 (1997) 1327–1330, http://dx.doi.org/10.1103/PhysRevLett.78.1327, URL https://link.aps.org/doi/10.1103/PhysRevLett.78.1327.
[39] L. Huang, S.J. Chey, J. Weaver, Metastable structures and critical thicknesses: Ag on Si(111)-7 × 7, Surf. Sci. 416 (1998) L1101– L1106, http://dx.doi.org/10.1016/S0039-6028(98)00627-X, URL http://www.sciencedirect.com/science/article/pii/S003960289800627X.
[40] I. Matsuda, T. Ohta, H.W. Yeom, In-plane dispersion of the quantum-well states of the epitaxial silver films on silicon, Phys. Rev. B 65 (2002) 085327, http://dx.doi.org/10.1103/PhysRevB.65.085327, URL https://link.aps.org/doi/10.1103/PhysRevB.65.085327.
[41] R. Flammini, F. Wiame, R. Belkhou, M. Marsi, L. Gregoratti, A. Barinov, M. Kiskinova, A. Taleb-Ibrahimi, Surf. Sci. 564 (2004) 121.
[42] K. Eguchi, Y. Takagi, T. Nakagawa, T. Yokoyama, Passivating effect of Si(111)-(root3xroot3)Ag and Si3N4/Si(111)-(8 × 8) buffer layers, J. Phys. Conf. Ser. 430 (2013) 012129, http://dx.doi.org/10.1088/1742-6596/430/1/012129.
[43] P. Allegrini, P. Sheverdyaeva, D. Trucchi, F. Ronci, S. Colonna, P. Moras, R. Flammini, A spectroscopy and microscopy study of silicon nanoclusters grown on β -Si3N4(0001)/Si(111) interface, Appl. Surf. Sci. 466 (2019) 59–62, http://dx.doi.org/10.1016/j.apsusc.2018.09.240, URL http://www.sciencedirect.com/science/article/pii/S0169433218326722.
[44] S. Yamauchi, M. Hirai, M. Kusaka, M. Iwami, H. Nakamura, Y. Yokota, A. Akiyama, H. Watabe, Ni-silicide formation: Dependence on crystallographic orientation of Si substrates, Japan. J. Appl. Phys. 32 (1993) 3237–3246, http://dx.doi.org/10.1143/jjap.32.3237.
[45] N. Nakajima, S. Hatta, J. Odagiri, H. Kato, Y. Sakisaka, Valence-band satellites in Ni: A photoelectron spectroscopic study, Phys. Rev. B 70 (2004) 233103, http://dx.doi.org/10.1103/PhysRevB.70.233103, URL https://link.aps.org/doi/10.1103/PhysRevB.70.233103.
[46] G.K. Wertheim, S.B. DiCenzo, D.N.E. Buchanan, Noble- and transition-metal clusters: The d bands of silver and palladium, Phys. Rev. B 33 (1986) 5384–5390, http://dx.doi.org/10.1103/PhysRevB.33.5384, URL https://link.aps.org/doi/10.1103/PhysRevB.33.5384.
[47] H.-M. Lee, C.-T. Kuo, H.-W. Shiu, C.-H. Chen, S. Gwo, Valence band offset and interface stoichiometry at epitaxial Si3N4/Si(111) heterojunctions formed by plasma nitridation, Appl. Phys. Lett. 95 (2009) 222104, http://dx.doi.org/10.1063/1.3269601.
[48] H. Ahn, C.-L. Wu, S. Gwo, C.M. Wei, Y.C. Chou, Structure determination of the Si_3N_4/Si(111)- (8 × 8) surface: A combined study of Kikuchi electron holography, scanning tunneling microscopy, and ab initio calculations, Phys. Rev. Lett. 86 (2001) 2818–2821, http://dx.doi.org/10.1103/PhysRevLett.86.2818, URL https://link.aps.org/doi/10.1103/PhysRevLett.86.2818.
[49] L. Aballe, C. Rogero, P. Kratzer, S. Gokhale, K. Horn, Probing interface electronic structure with overlayer quantum-well resonances: Al/Si(111), Phys. Rev. Lett. 87 (2001) 156801, http://dx.doi.org/10.1103/PhysRevLett.87.156801, URL https://link.aps.org/doi/10.1103/PhysRevLett.87.156801.
[50] D. Du Boulay, N. Ishizawa, T. Atake, V. Streltsov, K. Furuya, F. Munakata, Synchrotron X-ray and ab initio studies of β-Si3N 4, Acta Crystallogr. B 60 (2004) 388–405, http://dx.doi.org/10.1107/S010876810401393X, URL https://link.aps.org/doi/10.1103/PhysRevLett.87.156801.
[51] S. Nakanishi, T. Horiguchi, Related content surface lattice constants of Si (111), Ni (111) and, Japan. J. Appl. Phys. 20 (1981) 214–216, URL https://iopscience.iop.org/article/10.1143/JJAP.20.L214/meta.
[52] S.B. Mi, C.L. Jia, Q.T. Zhao, S. Mantl, K. Urban, NiSi2/Si interface chemistry and epitaxial growth mode, Acta Mater. 57 (2009) 232–236, http://dx.doi.org/10.1016/j.actamat.2008.09.002.
[53] A. Howie, Image contrast and localized signal selection techniques, J. Microsc. 117 (1979) 11–23.
[54] E.J. Kirkland, R.F. Loane, J. Silcox, Simulation of annular dark field STEM images using a modified multislice method, Ultramicroscopy 23 (1987) 77–96.
[55] S. Tulić, T. Waitz, O. Romanyuk, M. Varga, M. Čaplovičová, G. Habler, V. Vretenár, M. Kotlár, A. Kromka, B. Rezek, V. Skákalová, Ni-mediated reactions in nanocrystalline diamond on Si substrates: The role of the oxide barrier, RSC Adv. 10 (2020) 8224–8232, http://dx.doi.org/10.1039/d0ra00809e.
[56] F. Weitzer, J.C. Schuster, J. Solid State Chem. 70 (1987) 178.
[57] F. Edelman, E.Y. Gutmanas, A. Katz, R. Brener, Formation of nickel silicides in the Ni/Si3N4/Si system during rapid thermal annealing, Appl. Phys. Lett. 53 (1988) 1186–1188, http://dx.doi.org/10.1063/1.100665.
[58] R.R. Reeber, K. Wang, Thermal expansion and lattice parameters of group iv semiconductors, Mater. Chem. Phys. 46 (1996) 259–264, http://dx.doi.org/10.1016/S0254-0584(96)01808-1, URL https://www.sciencedirect.com/science/article/pii/S0254058496018081.
[59] T. Middelmann, A. Walkov, G. Bartl, R. Schödel, Thermal expansion coefficient of single-crystal silicon from 7 K to 293 K, Phys. Rev. B 92 (2015) 174113, http://dx.doi.org/10.1103/PhysRevB.92.174113, URL https://link.aps.org/doi/10.1103/PhysRevB.92.174113.
[60] A. Kuwabara, K. Matsunaga, I. Tanaka, Lattice dynamics and thermodynamical properties of silicon nitride polymorphs, Phys. Rev. B 78 (2008) 064104, http://dx.doi.org/10.1103/PhysRevB.78.064104, URL https://link.aps.org/doi/10.1103/PhysRevB.78.064104.
[61] F.C. Nix, D. MacNair, The thermal expansion of pure metals: Copper, gold, aluminum, nickel, and iron, Phys. Rev. 60 (1941) 597–605, http://dx.doi.org/10.1103/PhysRev.60.597, URL https://link.aps.org/doi/10.1103/PhysRev.60.597.
[62] B.H. Yu, D. Chen, Y.L. Jia, Pseudo-potential calculations of structural, elastic and thermal properties of Si3N4, in: High Performance Structures and Materials Engineering, in: Advanced Materials Research, vol. 217, Trans Tech Publications Ltd, 2011, pp. 1619–1624, http://dx.doi.org/10.4028/www.scientific.net/AMR.217-218.1619.
[63] I.C. Huseby, G.A. Slack, R.H. Arendt, Bull. Am. Ceram. Soc. 60 (1981) 919.
[64] R. Bruls, H. Hintzen, G. de With, R. Metselaar, J. van Miltenburg, The temperature dependence of the Grüneisen parameters of MgSiN2, AlN and β-Si3N4, J. Phys. Chem. Solids 62 (2001) 783–792, http://dx.doi.org/10.1016/S0022-3697(00)00258-4, URL https://www.sciencedirect.com/science/article/pii/S0022369700002584.

[65] L. Aballe, L. Gregoratti, A. Barinov, M. Kiskinova, T. Clausen, S. Gangopadhyay, J. Falta, Interfacial interactions at Au/Si3N4/Si(111) and Ni/Si3N4/Si(111) structures with ultrathin nitride films, Appl. Phys. Lett. 84 (2004) 5031–5033, http://dx.doi.org/10.1063/1.1763636.

[66] T. Nguyen, H.L. Ho, D.E. Kotecki, T.D. Nguyen, Reaction study of cobalt and silicon nitride, J. Mater. Res. 8 (1993) 2354–2361, http://dx.doi.org/10.1557/JMR.1993.2354.

[67] D.A. Zakheim, W.V. Lundin, A.V. Sakharov, E.E. Zavarin, P.N. Brunkov, E.Y. Lundina, A.F. Tsatsulnikov, S.Y. Karpov, Dependence of leakage current in Ni/Si3N4/n-GaN Schottky diodes on deposition conditions of silicon nitride, Semicond. Sci. Technol. 33 (2018) 115008, http://dx.doi.org/10.1088/1361-6641/aae242.